Geophysical Research Letters

RESEARCH LETTER
10.1029/2021GL097596

Key Points:

- Profiles from a long-duration balloon reveal equatorial waves with wide extent but very fine-vertical scales that are unresolved in models
- 97% of the cirrus clouds observed in the upper tropical tropopause layer (above 17 km) are related to these waves
- The analyzed waves provide strong QBO forces, pointing to a possible mechanism to improve the simulation of the QBO and its climate impacts

Correspondence to:
M. Bramberger,
martina@nwra.com

Citation:
Bramberger, M., Alexander, M. J., Davis, S., Podglajen, A., Hertzog, A., Kalnajs, L., et al. (2022). First super-pressure balloon-borne fine-vertical-scale profiles in the upper TTL: Impacts of atmospheric waves on cirrus clouds and the QBO. *Geophysical Research Letters*, *49*, e2021GL097596. https://doi.org/10.1029/2021GL097596

Received 23 DEC 2021
Accepted 24 FEB 2022

Author Contributions:
Conceptualization: Martina Bramberger, M. Joan Alexander
Data curation: Sean Davis, Albert Hertzog, Lars Kalnajs, Terry Deshler, J. Douglas Goetz, Sergey Khaykin
Formal analysis: Martina Bramberger
Funding acquisition: M. Joan Alexander, Lars Kalnajs, Terry Deshler, Sergey Khaykin
Investigation: Aurelien Podglajen
Methodology: Martina Bramberger, M. Joan Alexander, Sean Davis, Aurelien Podglajen, Albert Hertzog
Project Administration: M. Joan Alexander, Lars Kalnajs, J. Douglas Goetz
Software: Martina Bramberger
Supervision: M. Joan Alexander
Visualization: Martina Bramberger
Writing – original draft: Martina Bramberger, M. Joan Alexander

First Super-Pressure Balloon-Borne Fine-Vertical-Scale Profiles in the Upper TTL: Impacts of Atmospheric Waves on Cirrus Clouds and the QBO

Martina Bramberger[1], M. Joan Alexander[1], Sean Davis[2], Aurelien Podglajen[3], Albert Hertzog[3], Lars Kalnajs[4], Terry Deshler[4], J. Douglas Goetz[4], and Sergey Khaykin[5]

[1]NorthWest Research Associates, Boulder Office, Boulder, CO, USA, [2]NOAA Chemical Sciences Laboratory, Boulder, CO, USA, [3]Laboratoire de Météorologie Dynamique, École Polytechnique, Palaiseau, France, [4]Laboratory for Atmospheric and Space Physics, University of Colorado at Boulder, Boulder, CO, USA, [5]Laboratoire Atmosphères, Observations Spatiales (LATMOS), UVSQ, Sorbonne Université, CNRS, IPSL, Guyancourt, France

Abstract Atmospheric waves in the tropical tropopause layer are recognized as a significant influence on processes that impact global climate. For example, waves drive the quasi-biennial oscillation (QBO) in equatorial stratospheric winds and modulate occurrences of cirrus clouds. However, the QBO in the lower stratosphere and thin cirrus have continued to elude accurate simulation in state-of-the-art climate models and seasonal forecast systems. We use first-of-their-kind profile measurements deployed beneath a long-duration balloon to provide new insights into impacts of fine-scale waves on equatorial cirrus clouds and the QBO just above the tropopause. Analysis of these balloon-borne measurements reveals previously uncharacterized fine-vertical-scale waves (<1 km) with large horizontal extent (>1000 km) and multiday periods. These waves affect cirrus clouds and QBO winds in ways that could explain current climate model shortcomings in representing these stratospheric influences on climate. Accurately simulating these fine-vertical-scale processes thus has the potential to improve sub-seasonal to near-term climate prediction.

Plain Language Summary Instruments measuring temperature, water vapor, and ice particles were deployed on a 2-km-long string reeled up and down below a long-duration balloon drifting at 19 km in the lower stratosphere. The measurements reveal climate influences of very difficult-to-observe atmospheric waves with extreme aspect ratios: large horizontal scales (>1000 km) but very short vertical scales (<1 km). The waves are seen actively modifying properties of thin ice clouds that collectively influence tropical surface temperatures. An inverted Z-shape in the temperature profiles suggests these waves are intermittently breaking, like waves on a beach, leading to forces that drive zonal wind accelerations. The magnitude of these forces is strong, enough to drive the dominant zonal wind pattern called the Quasi-Biennial Oscillation (QBO), at least for the month-long period we observe. At these altitudes, the wave forces driving the QBO have been mysterious, despite world-wide efforts to simulate the QBO in climate models aiming to improve seasonal predictions.

1. Introduction

Tropical waves play a major role in driving large-scale atmospheric circulation (Baldwin et al., 2001) and generating cirrus clouds in the lower stratosphere (E. Jensen & Pfister, 2004; Kärcher et al., 2019; Kim et al., 2016; Schoeberl et al., 2015). These waves drive the quasi-biennial oscillation (QBO) in the zonal mean zonal wind in the lower stratosphere, and a growing body of evidence suggests that this oscillation is important to the intensity of the; Madden-Julian oscillation (MJO) in tropical precipitation (Lim et al., 2019; Marshall et al., 2017; Yoo & Son, 2016) and climate prediction at seasonal to interannual time scales (Garfinkel et al., 2018; Scaife et al., 2014; Smith et al., 2016). By lowering the cold point temperature in the tropical tropopause layer (TTL), these waves also play a role in limiting the amount of water vapor in the stratosphere (Fueglistaler et al., 2009; Kim & Alexander, 2015). Stratospheric water vapor has an important greenhouse effect with radiative impacts comparable to other greenhouse gases that influence the global surface temperature (Banerjee et al., 2019; Dessler et al., 2013; Forster & Shine, 2002; Solomon et al., 2010), and also constitutes an important climate feedback. Therefore, for climate prediction it is vital to realistically simulate the QBO, TTL cirrus clouds and water vapor in the stratosphere, and all three still pose considerable challenges for current models.

Writing – review & editing: Sean Davis, Aurelien Podglajen, Albert Hertzog, Lars Kalnajs, Terry Deshler

Tropical waves comprise small-scale convective gravity waves (CGWs) and equatorial-trapped modes including large-scale inertia-gravity waves (IGWs), mixed Rossby-gravity waves, Kelvin waves and Rossby waves. These waves have periods ranging from minutes to weeks and zonal wavelengths spanning orders of magnitude from 1 to 10,000 km. Particularly low-frequency IGW modes can pose a challenge for observations as their vertical wavelengths can become relatively very small, ≤1 km. Due to their fine vertical structure these waves are unresolved in current global circulation models (GCMs) despite their long horizontal wavelengths.

Fine-vertical-scale waves have consequences for modeling TTL cirrus clouds (Boehm & Verlinde, 2000; E. Jensen & Pfister, 2004; Kim et al., 2016; E. J. Jensen et al., 2016) as they can cool air in the upper TTL thus lowering entry values of stratospheric water vapor (Kim & Alexander, 2015; Schoeberl et al., 2015). Large-horizontal-scale waves can develop very fine-vertical-scales in certain QBO shear conditions (Holton et al., 2001; Vincent & Alexander, 2020). Particularly at lower stratospheric altitudes, where models most struggle to simulate realistic amplitude of the QBO (Bushell et al., 2020; Richter et al., 2020), unresolved fine-vertical-scale IGWs may be an important missing source of QBO forcing (Vincent & Alexander, 2020), and these lower stratospheric altitudes may be the most important region for simulating tropical stratospheric impacts on climate (Anstey et al., 2021).

Here, we use a unique data set collected during the Strateole-2 long-duration super-pressure balloon test campaign in 2019. During this campaign eight balloons were launched that circumnavigated Earth near the equator at flight altitudes ranging from 18 to 20 km (Haase et al., 2018; Corcos et al., 2021). We focus on balloon "TTL3" carrying a Thermodynamical SENsor (TSEN; Hertzog et al., 2004) instrument and the Reeldown Aerosol Cloud Humidity and Temperature Sensor (RACHuTS; Kalnajs et al., 2021). While the gondola TSEN measures temperature, pressure and horizontal wind at float level, RACHuTS provides high-resolution 2 km profiles of temperature, water vapor and aerosol at 1 m resolution below the balloon. We use these unique balloon measurements in conjunction with Constellation Observing System for Meteorology, Ionosphere, and Climate-2 (COSMIC-2) satellite observations and the fifth generation European Centre for Medium-Range Weather Forecasts (ECMWF) atmospheric reanalysis (ERA5), to provide for the first time, a classification of long-period waves with short vertical wavelengths and an assessment of their impact on cirrus clouds and the QBO in the lowermost tropical stratosphere.

2. Instruments and Datasets

The flight-level TSEN provides ambient air temperature and pressure measurements and GPS position at the isopycnic level of the drifting Strateole 2 balloon gondola. The TSEN data are available every 30 s. The temperature sensor accuracy is 0.1 K at night and 0.25 K during the day after correction for solar radiation (Hertzog et al., 2004). The absolute accuracy and precision of the pressure sensor are ±2 hPa and 0.01 hPa. Winds are derived from position with 0.1 ms^{-1} precision.

RACHuTS is a system designed to measure profiles down to 2 km below the flight level of a super pressure balloon (Kalnajs et al., 2021). It lowers and retracts an instrument package consisting of a TSEN temperature sensor, a water vapor sensor, and an aerosol spectrometer. The TSEN temperature sensor is a simplified version of the sensor described above. The water vapor sensor is a Fluorescence Lyman-Alpha Stratospheric Hygrometer (FLASH-B) and reports water vapor at 1 Hz with a precision of 5%–6% in the stratosphere, where the accuracy is limited by the calibration error of 4%. RACHuTS data are only collected at night where the solar zenith angle is >95° to ensure optimal sampling conditions for FLASH-B. The RACHuTS Optical Particle Counter uses Mie theory and side-scattered light by particles, from the laser illuminated sample stream, to measure the concentrations of the particles in eight size bins between 0.3 and 10 μm diameter. The concentrations of smallest particles, diameter >0.3 μm, are measured at 1 Hz, larger particles (0.5–10 μm) have an 8 s integration time. The upper size limit of the instrument is indefinite, all that can be determined is that a particle is larger than 10 µm. The sample flow rate is 3.5 L per minute.

Here we use the aerosol counter to identify the presence of ice particles. This is done using a size threshold of 3 μm. There are no instruments which can unambiguously identify ice at such small sizes, but as with numerous other studies we infer the presence of ice from measurements of particles with a size which is unlikely to appear at that altitude as a dry particle (Davis et al., 2010; Krämer et al., 2009, 2020; Thomas et al., 2002). For the RACHuTS profiles there are many observations of the size distribution of aerosol larger than 0.3 μm, and nearly

all instances of the presence of particles larger than 3, 5, and 10 μm are associated with conditions favorable for the existence of ice.

COSMIC-2 was launched in June 2019 and is a successor of the COSMIC mission launched in 2006 (Schreiner et al., 2020). It consists of six satellites orbiting Earth on a low geocentric orbit, that carry advanced Tri-GNSS (Global Navigation Satellite System) Radio Occultation receivers. We use COSMIC-2 dry temperature profiles that are valid from the upper troposphere up to 40 km provided at vertical resolution ~100 m with accuracy <0.1 K.

ERA5 is an atmospheric reanalysis provided by ECMWF (Hersbach et al., 2020). ERA5 data are available at 6 hr intervals on 137 levels up to 1 Pa with a horizontal resolution of 31 km. The distance between the different vertical levels is about 400 m in the lower stratosphere. We note that ERA5 might show significant errors in the equatorial lower stratosphere which is a challenging region for reanalysis (Podglajen et al., 2014).

3. Methods

3.1. Wave Temperature Perturbations in RACHuTS Profiles

For the calculation of wave temperature perturbations we use COSMIC-2 observations to derive background temperature profiles. A background profile is defined as an average in a box that is 5° × 10° latitude×longitude and 30 days in time. The box moves with the balloon along its flight track. The temperature perturbations from RACHuTS observations are calculated by subtracting the COSMIC-2 background temperature profile at the location and time of a RACHuTS profile. The perturbations so defined include waves with periods <30 days (Kim et al., 2016).

An adiabatic temperature profile gradient can be evidence for vertical mixing. Note that for temperature perturbations, the vertical gradient corresponding to an adiabatic lapse rate depends on the background temperature gradient $d\overline{T}/dz$ and can be written:

$$\left(\frac{dT'}{dz}\right)_{ad} = -\frac{g}{c_p} - \frac{d\overline{T}}{dz} \tag{1}$$

where g is the gravitational acceleration, c_p is the specific heat at constant pressure, $(dT'/dz)_{ad}$ is the temperature perturbation gradient that would make the total lapse rate adiabatic. Equation 1 is derived assuming that the total temperature lapse rate $-(dT/dz)_{ad}$ equals the adiabatic lapse rate such that,

$$\left(\frac{dT}{dz}\right)_{ad} = \frac{d\overline{T}}{dz} + \left(\frac{dT'}{dz}\right)_{ad} = -\frac{g}{c_p}. \tag{2}$$

$d\overline{T}/dz$ is derived from COSMIC2 background temperature profiles between 17 and 19 km altitude where RACHuTS profiles are available.

Wave vertical wavelengths will be key to identifying the type of wave. Due to the RACHuTS profile length, only waves with vertical wavelengths smaller than 2 km are fully resolved. Using a S-transform (Stockwell et al., 1996) spectral analysis we derive the vertical wavelengths from the RACHuTS profiles.

3.2. Calculation of Total Wave Energy

Because the super-pressure balloons drift with the ambient wind, analysis of the wind and temperature perturbations in the TSEN observations permit direct estimates of wave intrinsic periods. The perturbations from TSEN observations are calculated by subtracting a 30 days running mean value of the respective quantity. We decompose the total perturbation energy (E_{tot}) from the in situ observed wind and temperature perturbations along the flight track into time and frequency spectrum using the S-transform (Stockwell et al., 1996). The total energy spectrum is given by

$$E_{tot} = 0.5\left[\left(\hat{u}^2 + \hat{v}^2\right) + \frac{g^2}{N^2}\frac{\hat{T}^2}{\overline{T}}\right]. \tag{3}$$

N is the static stability, g the gravitational acceleration, $\overline{T}$ is the background temperature, $\hat{u}$ and $\hat{v}$ are the zonal and meridional wind amplitudes, and $\hat{T}$ the temperature amplitude.

3.3. Wave Momentum Flux and Drag Calculation

The drag force exerted on the atmosphere from IGWs is calculated as the divergence of momentum flux, or

$$F_{local} = -\frac{1}{\rho}\frac{d\left(\rho\overline{u'w'}\right)}{dz} \tag{4}$$

with the density ρ and the zonal momentum flux $\left(\rho\overline{u'w'}\right)$. While u' is calculated from TSEN observations, the vertical velocity perturbation, w', is derived from the wave vertical displacement, ξ' by

$$w' = i\hat{\omega}\xi' \tag{5}$$

where $\hat{\omega}$ is the intrinsic frequency and

$$\xi' = \frac{\xi'_b}{\alpha} \tag{6}$$

with $\alpha \approx 0.3$ and ξ'_b is the balloon vertical displacement (Corcos et al., 2021; Podglajen et al., 2016; Vincent & Alexander, 2020). ρ is calculated from COSMIC2. That way our momentum flux estimate is based on observations.

Due to uncertainty in deriving vertical velocity for inertia-gravity waves with extreme long periods (>2.5 days), we also estimate momentum flux with the "indirect method" of (Sato & Dunkerton, 1997) for comparison. Following (Sato & Dunkerton, 1997), $\overline{u'w'}$ associated with IGWs in QBO shear conditions is given by,

$$\overline{u'w'} = \frac{2g\omega}{N\bar{T}}\left(\frac{\delta u}{\delta z}\right)^{-1}\overline{u'T'} \tag{7}$$

where g is the gravitational acceleration, ω is the intrinsic frequency, N is the static stability, $\bar{T}$ is the mean temperature, $\frac{\delta u}{\delta z}$ is the vertical shear of zonal background wind and $\overline{u'T'}$ is the zonal heat flux calculated as cospectrum of zonal wind and temperature perturbations. The parameters N and $\bar{T}$ are derived from COSMIC-2 observations, and $\frac{\delta u}{\delta z}$ from ERA5, while ω and $\overline{u'T'}$ are calculated from TSEN measurements.

We assume the wave momentum flux will dissipate between the balloon observation level and the wave critical level.

Since the IGWs discussed in this study have limited zonal extent while QBO forcing is a zonal-mean concept, we estimate the zonal-mean drag of the IGWs by applying an area factor A to the local drag F_{local}

$$\bar{F}_{zonal} = F_{local} \times A \tag{8}$$

where overbars denote zonal means. Here, we assume A to be proportional to three times the zonal wavelength of the observed IGWs divided by Earth's circumference (Vincent & Alexander, 2020).

4. Results

We focus on the time period from 9 December 2019 to 9 January 2020 where the TTL3 balloon drifted in eastward QBO winds at 66 hPa from the Pacific across South America to the Atlantic Ocean toward Africa (Figure 1). This time period includes 30 RACHuTS profiles between 27 December and 5 January (4.5°N/172.4°W and 0.5°N/15.5°W).

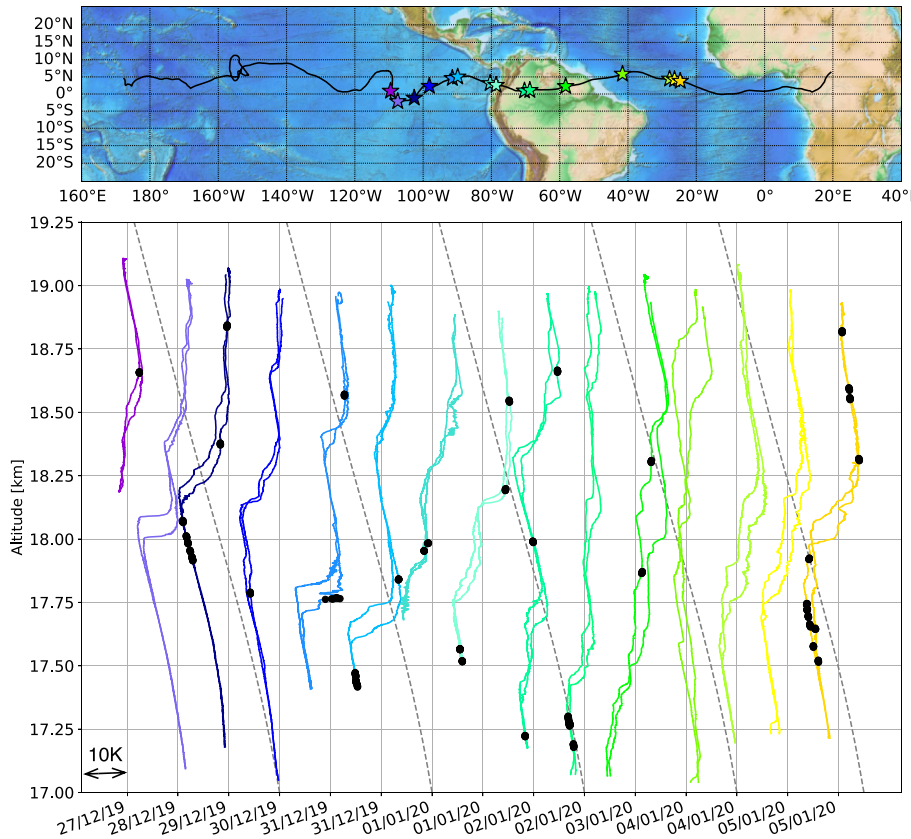

Figure 1. Flight track of the TTL3 balloon during the Strateole-2 campaign from 9 December to 9 January (upper panel). The stars show the positions of the pairs of descending/ascending RACHuTS temperature perturbation profiles shown in the lower panel. Each pair of RACHuTS profiles are separated by 10K. The color coding corresponds to the location of the profile (see map) and the date of the profile pair is given on the *x*-axis. The gray vertical lines highlight $T' = 0$ for each night's pair of profiles. Temperature perturbations are due to waves with periods <30 days. Black dots represent the location of ice observations and the black dashed lines show the slope of perturbations giving a net adiabatic lapse rate, indicating mixed layers. For reference the mean tropopause is near 17 km at 191K.

4.1. RACHuTS Observed Wave Amplitudes

The temperature perturbation (T') profiles derived from RACHuTS observations show signatures of large amplitude waves and evidence of turbulent mixing layers due to convective instability (see Figure 1). The measurements are primarily above the mean tropopause (defined by COSMIC-2 balloon-following background), which occurs at 17.2 ± 0.3 km with a temperature of 191 ± 3 K.

Many of the profiles exhibit a distinct inverted Z-shape with shallow positive vertical T' gradients above and below layers with near-adiabatic lapse rate of varying depths (e.g., 31 December 2019 with a depth of about 600 m). As also shown in (Podglajen et al., 2017), the near-adiabatic layers are related to the less stable $dT'/dz < 0$ phase of low frequency waves, and these layers are likely remnants of convective instability and turbulent mixing in the unstable phase of these waves. Unlike (Podglajen et al., 2017), our data permit analysis of wave type, frequency, and horizontal scale (Section 3.3), which suggest these mixed layers have wide horizontal extent.

4.2. Ice Clouds and Wave Interactions

The RACHuTS ice particle detections, defined by particle sizes >3 μm, are highlighted with black dots in Figure 1. The particle concentration in these regions is on the order of 3/L. On two occasions concentrations exceeded 6/L and in 20% of the cases 5 μm particles were also observed. Thus these are very thin clouds, invisible to remote sensors, and the ice particles grow slowly with a limited vapor supply. In several of the clouds,

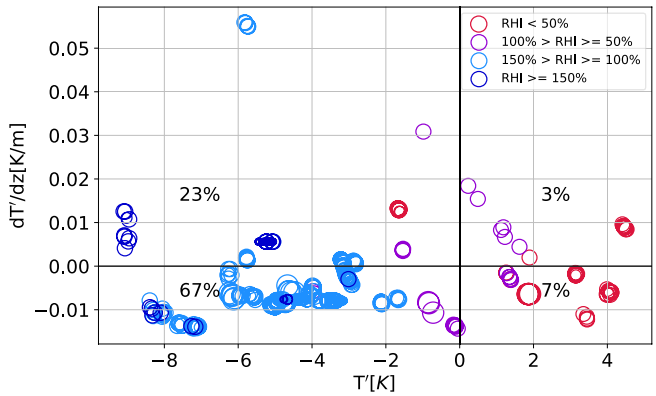

Figure 2. Wave influence on cirrus cloud detections at and around South America. The plot shows the distribution of particles ≥3 μm, considered to be ice, as a function of wave perturbations (T') and the vertical gradient of the temperature perturbation T' ($dT'/dz \sim dT'/dt$). The colors refer to relative humidity above ice (RHI) and the percentages given in the quadrants are the percentage of particles found in the respective quadrant relative to all particle counts. The circle sizes are proportional to particle concentrations where small circles represent 1/L, medium size circles 3/L and the largest circles 6/L.

the concentration of 2 µm particles was increased to 6–15/L, well above the bulk of aerosol concentrations at this size, indicating that these particles were probably also ice.

Previous studies have shown that ice cloud occurrences in the TTL are related to wave temperature changes (Chang & L'Ecuyer, 2020; Kim et al., 2016). The influence of waves on clouds is primarily determined not only by the cold ($T' < 0$) or warm ($T' > 0$) phase of the wave, but also by the wave-induced cooling rate, which is proportional to the change in phase with height dT'/dz (Kim et al., 2016; Podglajen et al., 2018). Following previous studies we evaluate ice cloud detections as a function of the four phases corresponding to positive or negative wave perturbations (T') and their vertical gradients dT'/dz proportional to cooling rate (Chang & L'Ecuyer, 2020; Kim et al., 2016), and as a function of ice relative humidity (Figure 2).

In concurrence with previous studies (Chang & L'Ecuyer, 2020; Kim et al., 2016) our analysis shows that 90% of sub visible cirrus cloud detections at upper TTL altitudes, above the mean cold point, occur in the cold phase of waves (left half of Figure 2). Most of the detections (67%) are in the cold phase of the wave while it is also actively cooling. Colors in Figure 2 show more extreme supersaturation occurs at larger negative wave perturbations, and supersaturation is rather less sensitive to the cooling rates. The strong relationships between ice cloud occurrence, extreme supersaturations, and waves raise the question, what types of waves are generating these sub visible clouds?

4.3. Wave Type Identification

Identifying the wave types will permit estimation of their horizontal scales and their effects on the QBO winds. In the time period of interest the balloon drifted in westerly QBO winds (Figure 3a). The wave energy spectrum per unit density E_{tot} (Figure 4, Equation 3) exhibits enhanced values at intrinsic periods of 2.5–5 days, and 11.5–15 days.

To provide further insight into the regions of enhanced E_{tot} (3), we use the RACHuTS vertical temperature perturbation profiles (Figure 1). We use the example of the 29 December 2019 to explain the analysis. The vertical wavelength derived from the observation on 29 December is 875 m. Assuming that the vertical RACHuTS profiles sample the waves observed with the in-situ TSEN measurements we use the dispersion relationships

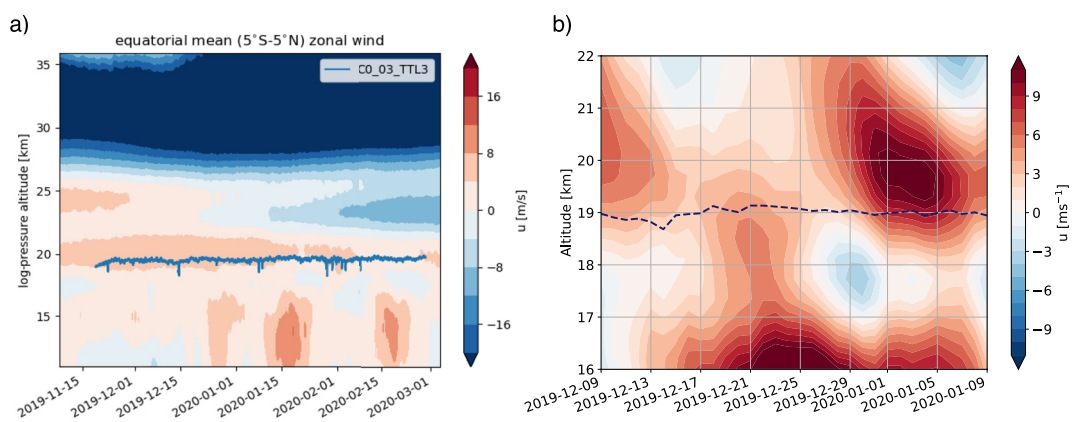

Figure 3. Equatorial zonal winds simulated by ERA5. (a) Time-height variations in zonal mean zonal wind averaged between 5°SN and 5°S with the balloon altitude (blue line). The zonal mean zonal wind shows the structure of the QBO above the tropopause. (b) Eight-day-running-mean zonal wind along the balloon flight-track as a function of altitude and time. The dark-blue dashed line shows the daily averaged altitude of the balloon.

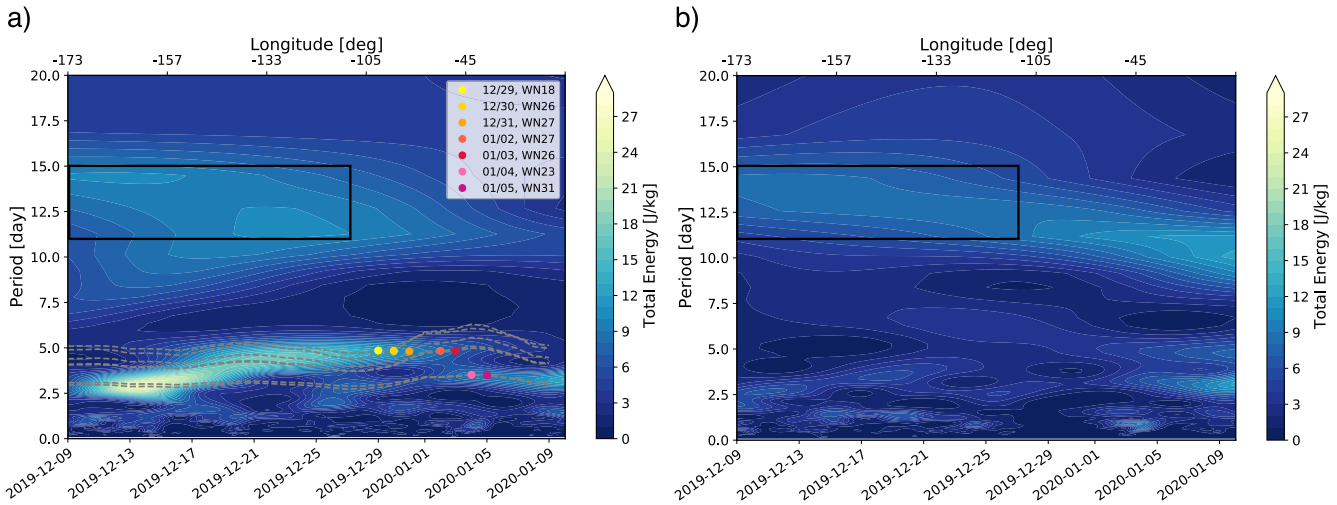

Figure 4. Wave energy spectrum E_{tot} (color shading) as a function of time and wave period from the balloon flight-level TSEN observations (a) and ERA5 (b). The color bar refers to E_{tot} and the gray dashed lines show the theoretical intrinsic period variations in time for eastward inertia gravity waves with zonal wavenumbers ranging from 15 to 28. The colored points in (a) highlight the starting points based on RACHuTS observed wavelengths from which the intrinsic periods have been calculated backwards and forwards in time. Periods and dates suggestive of Rossby waves are highlighted with a black box.

(Andrews et al., 1987) with the observed vertical wavelengths and the TSEN observed intrinsic periods to attribute the peaks in the total energy spectrum to specific wave types. Specifically, the peak at intrinsic period of 4.8 days on 29 December is identified as an $n = 0$ eastward propagating IGW (EIGW) with zonal wavenumber 18 (WN18; Kiladis et al., 2009). Considering all available RACHuTS profiles that are at least 1,200 m long (i.e., all profiles except 28 December and 1 January) we attribute the enhanced total energies to a $n = 0$ EIGW packet with wavenumbers ranging from ~18 to 27 (λ_h = 2,666 km–1,481 km) for the intrinsic period of 4.8 days and $n = 1$ WN23 and 31 EIGWs (λ_h = 1,739 km–1,290 km) for an intrinsic period of 3.5 days. The intrinsic phase speed of both wave packets is ~5 ms^{-1}.

So far we could attribute the enhanced total energy levels to specific wave types only for times where RACHuTS observations are available. To identify wave types outside the period covered with RACHuTS observations we need supplemental information from ERA5 analyses. Both, the observation (Figure 4a) and the ERA5 analyses (Figure 4b) exhibit elevated levels of total energy at periods 11.5–15 days from 9 December to 27 December (black box in 4). These energies are consistent with a $n = 1$ Rossby wave with a long vertical structure that is resolved in ERA5 reanalysis (Figure 4b). On the contrary EIGW energy at 2.5–5 days is strongly underestimated in ERA5, likely due to its too coarse vertical resolution.

To understand the elevated energy levels with intrinsic periods between 2.5 and 5 days outside the time-period of RACHuTS observations we calculate the Doppler-shift of wave intrinsic periods along the TTL3 flight track. For this analysis we use ERA5 zonal wind, smoothed over 8 days as background winds (Figure 3b) and linear wave theory (Andrews et al., 1987). The gray dashed lines in Figure 4a show the backward and forward evolution of intrinsic periods for the EIGW packets previously identified, based on the ERA5 background wind (Figure 3b). The colored dots highlight the respective starting dates and intrinsic periods. The Doppler shifted intrinsic periods starting between 29 December and 2 January align well with the evolution of the total energy peak between 17 December and about 2 January. Therefore, we associate shifts in enhanced energies with intrinsic periods from about 3.5 to 5 days in that time frame to Doppler shifted EIGWs with WN18–27. The Doppler shifted intrinsic periods starting on 4 and 5 of January connect well the enhanced total energies from 13 December to 5 January. As the intrinsic periods on 13 December are consistent with the wave properties observed between 5 and 9 January, we hypothesize that the elevated total energies on the 13 December 2019 are of similar wave type as observed on 4 and 5 January. This analysis highlights the widespread occurrence of EIGWs for intrinsic periods between 2.5 and 5 days.

We estimate the zonal mean force of the observed EIGWs ~0.3 ms^{-1} day^{-1} using Equation 5 and ~0.5 ms^{-1} day^{-1} using Equation 7. Both estimates are close to the magnitude of the total wave forcing necessary to drive the QBO

in models at these levels (Holt et al., 2016, 2020; Pahlavan et al., 2021). Considering the approximate ground-based phase speed of 12 ms^{-1} and the background zonal wind profile (Figure 3b) this forcing estimate is based on the assumption that the waves will encounter a critical level (c = u) within 1 km above the balloon flight track (see Figure 3b) and dissipate completely. The estimated forcing occurs at ∼19–20 km, which is near the bottom of the QBO, an important region where the QBO may impact surface climate and where most GCMs underestimate the variability in the QBO winds (Bushell et al., 2020).

5. Summary and Discussions

The measurements presented allow for the first time to identify large-scale waves with fine vertical scales as equatorial EIGWs in the upper TTL/lowermost stratosphere, and to determine their impact on cirrus clouds and QBO forcing.

5.1. Significance to Ice Clouds Modeling

Our analysis shows that 97% of the ice clouds observed were related to EIGW activity (see Figure 2). These cirrus clouds are extremely thin and subvisible to satellite observations. Previous observations have identified Kelvin wave influences on cirrus in the TTL (Boehm & Verlinde, 2000; Fujiwara et al., 2009; Holton et al., 2001), and theoretical studies stress the importance of high-frequency waves in the generation of cirrus clouds (E. Jensen & Pfister, 2004; Kärcher et al., 2019). The present observations add to these mechanisms the modulation of thin cirrus clouds by equatorial IGW with long horizontal wavelengths (1,000s of km) and short vertical wavelengths (<1 km). Including these equatorial IGWs may help explain the widespread occurrence of thin cirrus layers in the upper TTL.

The finding that the cold phase of these EIGWs generates ice suggests that they could be impacting the entry value of stratospheric water vapor through additional dehydration events as air ascends into the stratosphere if the environment remains supersaturated long enough to grow the ice crystals to sizes large enough to sediment out. In particular, the fact that the EIGW-generated clouds occur near and above the climatological cold point tropopause (∼380K) with periods of 2–5 days means that they could be dehydrating air masses that would otherwise not undergo further dehydration (all RACHuTS-measured clouds occurred above 373K). However, it is impossible with the present study to quantify potential contribution of EIGWs to stratospheric water vapor, and additional measurements are needed to quantify whether this contribution is significant.

5.2. Implications for Simulating the QBO

The EIGWs detected herein are characterized by very long horizontal scales, but very short vertical scales at and below the vertical resolution of modern GCMs and satellite observations. Our estimate of the contribution of the EIGWs to the forcing of the QBO is substantial as it is comparable to the total forcing of the QBO at lowermost stratosphere levels (Holt et al., 2016). At the observed EIGW breaking altitudes, GCMs consistently underestimate the amplitude of the QBO (Bushell et al., 2020). Comparison of total energy spectra from flight-level TSEN observations and ERA5 shows that these types of waves are missing even in state-of-the-art reanalysis (Figure 4). Therefore, the models also miss the forcing exerted by short-vertical wavelength IGWs in the lowermost stratosphere, and these waves might be key for the realistic simulation of the QBO and its interaction with the MJO in the lowermost stratosphere.

Data Availability Statement

Strateole-2 data is available on https://data.ipsl.fr/catalog/strateole2/ including RACHuTS data. COSMIC-2 data was downloaded from https://data.cosmic.ucar.edu/gnss-ro/cosmic2/nrt/level2/2019/ and https://data.cosmic.ucar.edu/gnss-ro/cosmic2/nrt/level2/2020/. ERA5 is available on https://apps.ecmwf.int/data-catalogues/era5/?type=an&class=ea&stream=oper&expver=1.

Acknowledgments
We thank Robert Vincent for helpful discussions about waves in superpressure balloon data. The TSEN and RACHuTS data were collected as part of Strateole-2, which is sponsored by CNES, CNRS/INSU and NSF. Joan Alexander and Martina Bramberger were supported by NSF grants 1642246 and 1642644. The RACHuTS measurements were completed under support from NSF award 1643022. We thank two anonymous reviewers for their helpful comments.

References

Andrews, D. G., Holton, J. R., & Leovy, C. B. (1987). *Middle atmosphere dynamics*.
Anstey, J. A., Simpson, I. R., Richter, J. H., Naoe, H., Taguchi, M., Serva, F., et al. (2021). Teleconnections of the quasi-biennial oscillation in a multi-model ensemble of QBO-resolving models. *Quarterly Journal of the Royal Meteorolgical Society*, 1–25. https://doi.org/10.1002/qj.4048
Baldwin, M. P., Gray, L. J., Dunkerton, T. J., Hamilton, K., Haynes, P. H., Randel, W. J., et al. (2001). The quasi-biennial oscillation. *Reviews of Geophysics*, *39*(2), 179–229. https://doi.org/10.1029/1999RG000073
Banerjee, A., Chiodo, G., Previdi, M., Ponater, M., Conley, A., & Polvani, L. (2019). Stratospheric water vapor: An important climate feedback. *Climate Dynamics*, *53*, 1697–1710. https://doi.org/10.1007/s00382-019-04721-4
Boehm, M. T., & Verlinde, J. (2000). Stratospheric influence on upper tropospheric tropical cirrus. *Geophysical Research Letters*, *27*(19), 3209–3212. https://doi.org/10.1029/2000GL011678
Bushell, A. C., Anstey, J. A., Butchart, N., Kawatani, Y., Osprey, S. M., Richter, J. H., et al. (2020). Evaluation of the Quasi-Biennial Oscillation in global climate models for the SPARC QBO-initiative. *Quarterly Journal of the Royal Meteorolgical Society*. https://doi.org/10.1002/qj.3765
Chang, K.-W., & L'Ecuyer, T. (2020). Influence of gravity wave temperature anomalies and their vertical gradients on cirrus clouds in the tropical tropopause layer – A satellite-based view. *Atmospheric Chemistry and Physics*, *20*(21), 12499–12514. https://doi.org/10.5194/acp-20-12499-2020
Corcos, M., Hertzog, A., Plougonven, R., & Podglajen, A. (2021). Observation of gravity waves at the tropical tropopause using superpressure balloons. *Journal of Geophysical Research Atmospheres*, *126*(15), e2021JD035165. https://doi.org/10.1029/2021JD035165
Davis, S., Hlavka, D., Jensen, E., Rosenlof, K., Yang, Q., Schmidt, S., et al. (2010). In situ and lidar observations of tropopause subvisible cirrus clouds during TC4. *Journal of Geophysical Research Atmospheres*, *115*(D10). https://doi.org/10.1029/2009JD013093
Dessler, A. E., Schoeberl, M. R., Wang, T., Davis, S. M., & Rosenlof, K. H. (2013). Stratospheric water vapor feedback. *Proceedings of the National Academy of Sciences*, *110*, 18087–18091. https://doi.org/10.1073/pnas.1310344110
Forster, P. M. d. F., & Shine, K. P. (2002). Assessing the climate impact of trends in stratospheric water vapor. *Geophysical Research Letters*, *29*(6), 10–1104. https://doi.org/10.1029/2001GL013909
Fueglistaler, S., Dessler, A. E., Dunkerton, T. J., Folkins, I., Fu, Q., & Mote, P. W. (2009). Tropical tropopause layer. *Reviews of Geophysics*, *47*(1). https://doi.org/10.1029/2008RG000267
Fujiwara, M., Iwasaki, S., Shimizu, A., Inai, Y., Shiotani, M., Hasebe, F., et al. (2009). Cirrus observations in the tropical tropopause layer over the western Pacific. *Journal of Geophysical Research Atmospheres*, *114*(D9). https://doi.org/10.1029/2008JD011040
Garfinkel, C. I., Schwartz, C., Domeisen, D. I. V., Son, S.-W., Butler, A. H., & White, I. P. (2018). Extratropical atmospheric predictability from the quasi-biennial oscillation in subseasonal forecast models. *Journal of Geophysical Research Atmospheres*, *123*(15), 7855–7866. https://doi.org/10.1029/2018JD028724
Haase, J., Alexander, M., Hertzog, A., Kalnajs, L., Deshler, T., Davis, S., et al. (2018). Around the world in 84 days. *EOS*, *99*. https://doi.org/10.1029/2018EO091907
Hersbach, H., Bell, B., Berrisford, P., Hirahara, S., Horányi, A., Muñoz Sabater, J., et al. (2020). The ERA5 global reanalysis. *Quarterly Journal of the Royal Meteorolgical Society*, *146*(730), 1999–2049. https://doi.org/10.1002/qj.3803
Hertzog, A., Basdevant, C., Vial, F., & Mechoso, C. R. (2004). The accuracy of stratospheric analyses in the northern hemisphere inferred from long-duration balloon flights. *Quarterly Journal of the Royal Meteorological Society*, *130*(597), 607–626. https://doi.org/10.1256/qj.03.76
Holt, L. A., Alexander, M. J., Coy, L., Molod, A., Putman, W., & Pawson, S. (2016). Tropical waves and the quasi-biennial oscillation in a 7-km global climate simulation. *Journal of the Atmospheric Sciences*, *73*(9), 3771–3783. https://doi.org/10.1175/JAS-D-15-0350.1
Holt, L. A., Lott, F., Garcia, R. R., Kiladis, G. N., Cheng, Y.-M., Anstey, J. A., et al. (2020). An evaluation of tropical waves and wave forcing of the QBO in the QBOi models. *Quarterly Journal of the Royal Meteorological Society*. https://doi.org/10.1002/qj.3827
Holton, J. R., Alexander, M. J., & Boehm, M. T. (2001). Evidence for short vertical wavelength Kelvin waves in the Department of Energy-Atmospheric Radiation Measurement Nauru99 radiosonde data. *Journal of Geophysical Research Atmospheres*, *106*(D17), 20125–20129. https://doi.org/10.1029/2001JD900108
Jensen, E., & Pfister, L. (2004). Transport and freeze-drying in the tropical tropopause layer. *Journal of Geophysical Research Atmospheres*, *109*(D2). https://doi.org/10.1029/2003JD004022
Jensen, E. J., Ueyama, R., Pfister, L., Bui, T. V., Alexander, M. J., Podglajen, A., et al. (2016). High-frequency gravity waves and homogeneous ice nucleation in tropical tropopause layer cirrus. *Geophysical Research Letters*, *43*(12), 6629–6635. https://doi.org/10.1002/2016GL069426
Kalnajs, L. E., Davis, S. M., Goetz, J. D., Deshler, T., Khaykin, S., St Clair, A., et al. (2021). A reel-down instrument system for profile measurements of water vapor, temperature, clouds, and aerosol beneath constant-altitude scientific balloons. *Atmospheric Measurement Techniques*, *14*(4), 2635–2648. https://doi.org/10.5194/amt-14-2635-2021
Kärcher, B., Jensen, E. J., & Lohmann, U. (2019). The impact of mesoscale gravity waves on homogeneous ice nucleation in cirrus clouds. *Geophysical Research Letters*, *46*(10), 5556–5565. https://doi.org/10.1029/2019GL082437
Kiladis, G. N., Wheeler, M. C., Haertel, P. T., Straub, K. H., & Roundy, P. E. (2009). Convectively coupled equatorial waves. *Reviews of Geophysics*, *47*(2). https://doi.org/10.1029/2008RG000266
Kim, J.-E., & Alexander, M. J. (2015). Direct impacts of waves on tropical cold point tropopause temperature. *Geophysical Research Letters*, *42*(5), 1584–1592. https://doi.org/10.1002/2014GL062737
Kim, J.-E., Alexander, M. J., Bui, T. P., Dean-Day, J. M., Lawson, R. P., Woods, S., et al. (2016). Ubiquitous influence of waves on tropical high cirrus clouds. *Geophysical Research Letters*, *43*(11), 5895–5901. https://doi.org/10.1002/2016GL069293
Krämer, M., Rolf, C., Spelten, N., Afchine, A., Fahey, D., Jensen, E., et al. (2020). A microphysics guide to cirrus – Part 2: Climatologies of clouds and humidity from observations. *Atmospheric Chemistry and Physics*, *20*(21), 12569–12608. https://doi.org/10.5194/acp-20-12569-2020
Krämer, M., Schiller, C., Afchine, A., Bauer, R., Gensch, I., Mangold, A., et al. (2009). Ice supersaturations and cirrus cloud crystal numbers. *Atmospheric Chemistry and Physics*, *9*(11), 3505–3522. https://doi.org/10.5194/acp-9-3505-2009
Lim, Y., Son, S.-W., Marshall, A. G., Hendon, H. H., & Seo, K.-H. (2019). Influence of the QBO on MJO prediction skill in the subseasonal-to-seasonal prediction models. *Climate Dynamics*, *53*(3), 1681–1695. https://doi.org/10.1007/s00382-019-04719-y
Marshall, A., Hendon, H., Son, S.-W., & Lim, Y. (2017). Impact of the quasi-biennial oscillation on predictability of the Madden–Julian oscillation. *Climate Dynamics*, *0849*. https://doi.org/10.1007/s00382-016-3392-0
Pahlavan, H. A., Fu, Q., Wallace, J. M., & Kiladis, G. N. (2021). Revisiting the quasi-biennial oscillation as seen in ERA5. Part I: Description and momentum budget. *Journal of the Atmospheric Sciences*, *78*(3), 673–691. https://doi.org/10.1175/JAS-D-20-0248.1
Podglajen, A., Bui, T. P., Dean-Day, J. M., Pfister, L., Jensen, E. J., Alexander, M. J., et al. (2017). Small-scale wind fluctuations in the tropical tropopause layer from aircraft measurements: Occurrence, nature, and impact on vertical mixing. *Journal of the Atmospheric Sciences*, *74*(11), 3847–3869. https://doi.org/10.1175/JAS-D-17-0010.1

Podglajen, A., Hertzog, A., Plougonven, R., & Legras, B. (2016). Lagrangian temperature and vertical velocity fluctuations due to gravity waves in the lower stratosphere. *Geophysical Research Letters*, *43*(7), 3543–3553. https://doi.org/10.1002/2016GL068148

Podglajen, A., Hertzog, A., Plougonven, R., & Žagar, N. (2014). Assessment of the accuracy of (re)analyses in the equatorial lower stratosphere. *Journal of Geophysical Research Atmospheres*, *119*(1911), 11,166–11,188. https://doi.org/10.1002/2014JD021849

Podglajen, A., Plougonven, R., Hertzog, A., & Jensen, E. (2018). Impact of gravity waves on the motion and distribution of atmospheric ice particles. *Atmospheric Chemistry and Physics*, *18*(14), 10799–10823. https://doi.org/10.5194/acp-18-10799-2018

Richter, J. H., Butchart, N., Kawatani, Y., Bushell, A. C., Holt, L., Serva, F., et al. (2020). Response of the Quasi-Biennial Oscillation to a warming climate in global climate models. *Quarterly Journal of the Royal Meteorolgical Society*, 1–29. https://doi.org/10.1002/qj.3749

Sato, K., & Dunkerton, T. J. (1997). Estimates of momentum flux associated with equatorial kelvin and gravity waves. *Journal of Geophysical Research Atmospheres*, *102*(D22), 26247–26261. https://doi.org/10.1029/96JD02514

Scaife, A. A., Athanassiadou, M., Andrews, M., Arribas, A., Baldwin, M., Dunstone, N., et al. (2014). Predictability of the quasi-biennial oscillation and its northern winter teleconnection on seasonal to decadal timescales. *Geophysical Research Letters*, *41*(5), 1752–1758. https://doi.org/10.1002/2013GL059160

Schoeberl, M. R., Jensen, E. J., & Woods, S. (2015). Gravity waves amplify upper tropospheric dehydration by clouds. *Earth and Space Science*, *2*(12), 485–500. https://doi.org/10.1002/2015EA000127

Schreiner, W., Weiss, J., Anthes, R., Braun, J., Chu, V., Fong, J., et al. (2020). COSMIC-2 Radio occultation constellation: First results. *Geophysical Research Letters*, *47*(4), e2019GL086841. https://doi.org/10.1029/2019GL086841

Smith, D. M., Scaife, A. A., Eade, R., & Knight, J. R. (2016). Seasonal to decadal prediction of the winter north Atlantic oscillation: Emerging capability and future prospects. *Quarterly Journal of the Royal Meteorological Society*, *142*(695), 611–617. https://doi.org/10.1002/qj.2479

Solomon, S., Rosenlof, K., Portmann, R., Daniel, J., Davis, S., Sanford, T., & Plattner, G.-K. (2010). Contributions of stratospheric water vapor to decadal changes in the rate of global warming. *Science*, *327*, 1219–1223. https://doi.org/10.1126/science.1182488

Stockwell, R. G., Mansinha, L., & Lowe, R. P. (1996). Localization of the complex spectrum: The S transform. *IEEE Transactions on Signal Processing*, *44*(4), 998–1001. https://doi.org/10.1109/78.492555

Thomas, A., Borrmann, S., Kiemle, C., Cairo, F., Volk, M., Beuermann, J., et al. (2002). In situ measurements of background aerosol and subvisible cirrus in the tropical tropopause region. *Journal of Geophysical Research Atmospheres*, *107*(D24). AAC8-1–AAC8-14. https://doi.org/10.1029/2001JD001385

Vincent, R. A., & Alexander, M. J. (2020). Balloon-borne observations of short vertical wavelength gravity waves and interaction with QBO winds. *Journal of Geophysical Research Atmospheres*, *125*(15), e2020JD032779. https://doi.org/10.1029/2020JD032779

Yoo, C., & Son, S.-W. (2016). Modulation of the boreal wintertime Madden-Julian oscillation by the stratospheric quasi-biennial oscillation. *Geophysical Research Letters*, *43*(3), 1392–1398. https://doi.org/10.1002/2016GL067762